JOURNAL OF AIRCRAFT
Vol. 39, No. 5, September–October 2002

Formation of a Rotor Tip Vortex

Hui Li,* O. R. Burggraf,† and A. T. Conlisk‡
Ohio State University, Columbus, Ohio 43210-1107

The origin of the tip vortex is described and important properties, such as core radius and circulation, as a function of these parameters, are calculated. Despite the fact that a large amount of computational and experimental work on the rotor wake has been published, little of a quantitative nature is known about the origin of the main component of the rotor wake, the tip vortex, as a function of the rotor speed, rotor blade geometry, and angle of attack. Experimental data by several workers have revealed little dependence on the Reynolds number. This lack of dependence on Reynolds number will hold only if the flow remains substantially unseparated, although it may be noted that drag coefficients of bluff bodies are remarkably constant over wide range of Reynolds number. The rotor blade is assumed to be of large aspect ratio, that is, to leading order in the blade aspect ratio, it appears infinite in length. In this limit case, the analytical solution for the bound circulation on a fixed wing is shown to be extendable to the rotary wing case when the blade is viewed as a lifting line. Lifting-surface results are obtained also, and these compare well with the lifting-line results for the bound circulation.

Introduction

THE helicopter-rotor wake is among the most complex flowfields in aerodynamics. The wake is fully three dimensional, and in many cases, there are regions within the wake in which the flow is extremely irregular.[1,2] Moreover, many experiments have focused on trimmed conditions in forward flight, which involves cyclic pitch, complicating the wake and making difficult fundamental experiments designed to elucidate primary wake features. It is well known that the wake position is difficult and expensive to calculate accurately beyond about one revolution of the rotor,[3,4] even using advanced computational fluid dynamics methods. Note that correlation of experimental data by other authors[5,6] has revealed little dependence on the Reynolds number, provided the flow remains substantially unseparated. Therefore, in this paper inviscid methods are used to describe the origin and evolution of the tip vortex, with the further goal of predicting circulation and local blade loads accurately.

Although there have been many papers that have presented results for the bound circulation on a rotor blade, there are relatively few papers that have addressed the physics of the formation of the tip vortex on rotor blades. Rule and Bliss[7] discuss the relationship between blade loading parameters and the tip-vortex circulation for a vortex with a turbulent core using a momentum integral approach. Bhagwat and Leishman[6] measured the velocity field near a rotor blade and used the data to integrate numerically around the blade at a specific spanwise location to obtain the bound circulation. They found that their results for a one-bladed rotor are independent of contour size, but the results for a two-bladed rotor are not. This discrepancy was explained by postulating that extraneous vorticity from the rotor wake was being included in the calculation. Even though the bound circulation results for the two-bladed rotor could not be made contour independent, they suggest that the strength of the tip vortex is about 83–85% of the maximum bound circulation. Earlier, Cook[8] presented experimental results suggesting that the tip-vortex circulation is much less than the maximum-bound circulation. In contrast, the experimental results of Caradonna and Tung[9] suggest that the tip-vortex circulation is close to the maximum.

In a comprehensive experiment, McAlister et al.[10] measured the fully three-dimensional velocity field for a rigid rotor blade; the measurements include data from as close as 0.3 chord length downstream of the trailing edge and so the origin of the tip vortex, in particular, can be analyzed. According to McAlister et al.,[10] the vortex begins to be formed near the point of maximum thickness on the top of the blade, and the center of the vortex is offset inboard a small amount. The vortex leaves the wing in the chordwise direction parallel to the trailing edge of each airfoil section, as is the case, in theory, when the classical Kutta condition is applied.

In this paper, we calculate the leading-order solution for the bound vorticity and its corresponding trailing vorticity for rotary wings; from these results the circulation of the tip vortex can be calculated. We then compare the results with existing experimental data. From an analytical and computational perspective, the flow near the tip has been viewed as the inner solution in a matched asymptotic expansion in the small parameter defined as the ratio of the chord to length of the rotor blade, that is, the inverse of the wing aspect ratio. This idea is not new: Van Dyke[11,12] alluded to this in his discussion of the fixed wing. For that case, Stewartson[13] derived an analytical formula for the bound circulation on a semi-infinite fixed wing. We have shown that a modified form of this formula is applicable to the rotor wing as well.

The configuration for our analysis is shown on Fig. 1, together with the subdivision into inner and outer regions. Consider the case of a fixed wing. Far from the tip, the circulation in the inner (tip) region becomes constant, and, to leading order, vorticity is not shed from the wing in that region. This observation explains the importance of the trailing vortices in the tip region and their relative unimportance inboard for a fixed wing. In the tip region where the circulation varies rapidly, the individual vortex filaments would be expected to roll over each other to form the tip vortex. In the case of the rotary wing, vorticity is shed inboard, and the bound circulation assumes a more or less linear behavior away from the blade tip. Later we show that Stewartson's solution[13] applies to the rotary wing as well, except that the rotary wing equation for the bound circulation involves an additional parameter, which is dependent on aspect ratio, angle of attack, and number of blades.

The formation of the tip vortex is viewed here as a collection of individual vortex filaments shed from discrete positions on the wing as a result of the spanwise variation of the bound circulation. The individual filaments roll around each other to form the tip vortex as shown in the photograph in Fig. 2 (Refs. 14, 15); these

Received 16 March 2001; revision received 15 March 2002; accepted for publication 15 April 2002.

*Graduate Research Associate, Department of Mechanical Engineering; currently Graduate Research Assistant, Computer Science Department, University of Arizona, Tucson, Arizona 85719.

†Professor Emeritus, Department of Aerospace Engineering and Aviation.

‡Professor, Department of Mechanical Engineering. Associate Fellow AIAA.

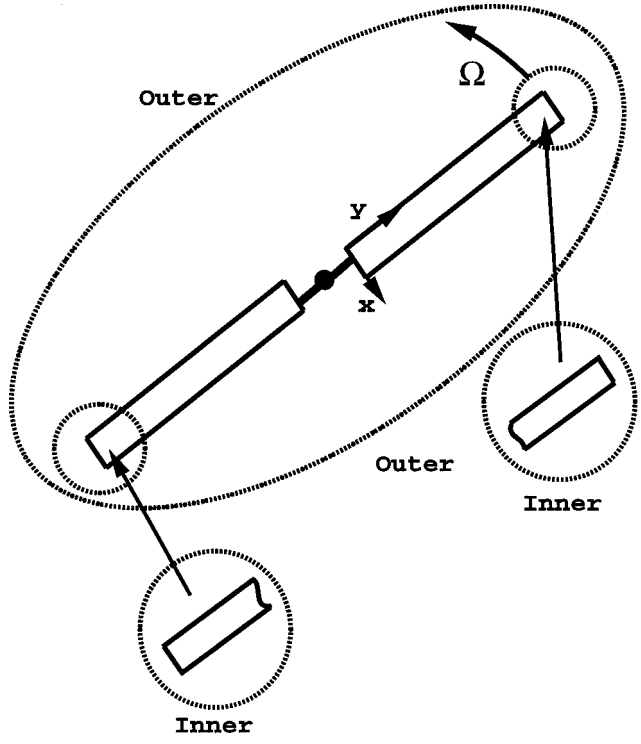

Fig. 1 Inner and outer problems for the flow past a two-bladed rotor.

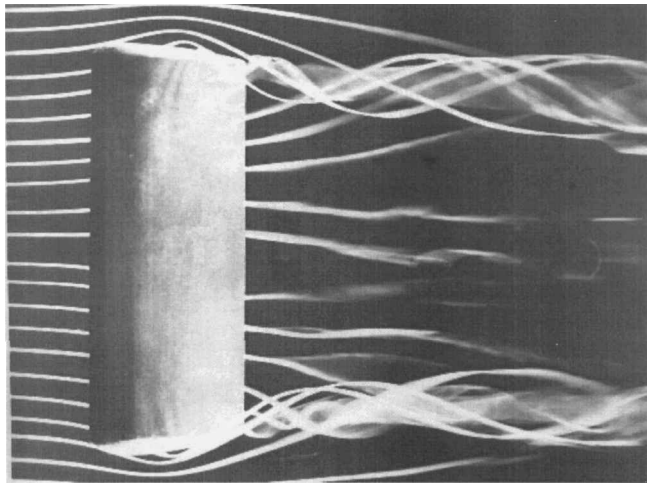

Fig. 2 Vortex wake of a fixed wing as photographed by Head.[14]

streakline patterns show the behavior of trailing vortices shed from discrete positions. Note that some of the vortexlike lines wrap from the underside. As quoted by Anderson,[16] such a filamentlike structure for the tip vortex is mentioned by Lanchester in Aerodynamics, published in 1907, indicating a long history of this interpretation. Lanchester shows a tip vortex as consisting of individual vortex filaments winding around themselves to form the developed tip vortex downstream.

The plan of the paper is as follows. After a discussion of the wake model, the lifting-surface problem is formulated. It is then found that, to leading order in aspect ratio, the blade appears semi-infinite in length. Horseshoe vortices are used to model the rotor blade and wake (inner problem), and the helical vortex structure of the far wake (outer problem) is modeled as a cylindrical structure of vortex rings. The numerical results for the circulation compare very well with the analytical solution for the rotary wing, corresponding to the lifting line. Results are then presented for the rollup structure of the tip vortex. Finally, a computational model for wake contraction is presented. The computational results for the bound circulation compare well with the experimental data for the rotary wing.

Asymptotics of Lifting-Line and Lifting-Surface Theory for Rotary Wing in Hover

Lifting Line

The integral equation of lifting-line theory has been derived for the case of a fixed wing in many text books. In particular, in Ref. 17,

$$\Gamma^*(y^*) = \frac{mc}{2}\left(U_\infty \alpha_0 - \frac{1}{4\pi}\int_{-b/2}^{b/2} \frac{\mathrm{d}\Gamma^*}{\mathrm{d}y_0^*}\frac{\mathrm{d}y_0^*}{y^* - y_0^*}\right) \tag{1}$$

where Γ^* is the circulation, α_0 is the geometric angle of attack, U_∞ is the speed far from the wing, b is the span of the wing, and c is the local value of the chord. Here m is a constant equivalent to the lift-curve slope, which is airfoil dependent. For a flat plate, $m = 2\pi$. In the general case, both c and α_0 may depend on y. It is important to understand the assumptions of linearized theory associated with the derivation of this equation. The following two points are of principal importance for our purposes.

1) The trailing wake is assumed to remain in the plane of the wing $z = 0$ for all time, or equivalently, in linearized theory, in the cross plane containing the freestream velocity vector.

2) The pressure difference between the bottom and the top of the wing must approach zero at the tip, and so $\Gamma^* = 0$ there also.

However, for a rotary wing, the trailing vortices are driven downward away from the rotor-tip path plane and form a more-or-less helical wake. Therefore, the assumption that trailing vortices remain in the rotor-tip path plane as for the fixed wing is not valid, and the lifting-line Eq. (1) can not be applied to the rotor tip directly. When the influence of the helical rotor wake is included, it is shown here that in the tip region, to leading order, the bound circulation of the rotary wing has a solution similar to that of a fixed wing, although the rotary wing analysis involves a parameter dependent on the aspect ratio, the angle of attack, and the number of blades.

We have applied the results of vortex theory together with the concepts of Prandtl's lifting-line theory to describe the interaction between an assumed cylindrical slipstream and the bound circulation for an n-bladed rotor operating in hover (static thrust). In Prandtl's theory, the high aspect ratio wing is represented by a line vortex (the lifting line), and the aerodynamic properties of each spanwise section are approximated locally by the two-dimensional characteristics from linearized airfoil theory. However, the freestream of the local section is replaced by the relative wind, that is, the effective angle of attack is the geometric angle of attack reduced by the local downwash induced by the trailing vortices.

For the case of the rotor blade in hover, two modifications must be made.

1) The true freestream in wing theory is replaced by the angular velocity of rotation of the blade.

2) The trailing vortices of the rotor follow a more-or-less helical path.

Corresponding to the variation of bound circulation, vortices are shed all across the rotor, forming an approximately cylindrical slipstream filled with concentric helical vortices. These discrete helical vortices are approximated by uniform cylindrical sheets of vorticity. For purposes of computing the downwash, these elemental vortex cylinders may be viewed as composed of vortex rings, whose strength is approximately constant on each cylinder. The axial component of the helical vortices, that is, the component of the circulation oriented in a direction normal to the tip-path plane may be ignored for present purpose because it does not contribute to the downwash.

A cylindrical coordinate system (r, θ, z) is convenient, where r is the radial coordinate, θ the azimuthal coordinate, and z the axial coordinate. (See Fig. 3, which illustrates a single vortex cylinder.) These elemental vortex cylinders, formed from the inboard vortex sheet, are superposed with the vortex cylinder generated by the tip vortex to form the complete rotor slipstream.

Unlike the apparently simpler case of the fixed wing, simple analytical formulas have been derived for rotor aerodynamics. Knight and Heffner[18] based their derivation on vortex theory, discussed earlier, whereas Gessow and Myers[19] derive the same result on the basis

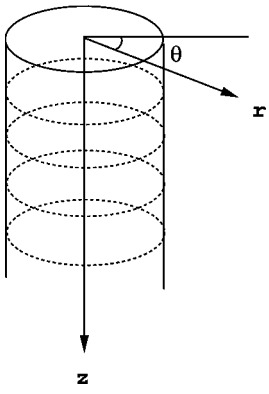

Fig. 3 Vortex-cylinder coordinate system.

of Glauert's[20] simple momentum theory. In either case, the results are shown to depend on a single parameter

$$\lambda = \epsilon\alpha_0 a/nc$$

where a is the blade-tip radius and n is the number of blades. For the case of a rectangular blade, the induced downwash has the form

$$W(R) = v_z/\Omega a\alpha_0 = (1/4\lambda)\left(\sqrt{1+8\lambda R}-1\right) \tag{2}$$

where $W(R)$ is the nondimensional downwash and $R = r/a$. We have introduced the parameter ϵ to account for the varying pitch of the helical vortex loops along the assumed cylindrical slipstream. Knight and Heffner[18] have taken $\epsilon = 2$, corresponding to conditions either just inside the slipstream boundary, or at infinity on the boundary itself, whereas $\epsilon = 1$ corresponds to conditions on the slipstream boundary just below the rotor. We have chosen $\epsilon = 1$ as more appropriate for evaluating the bound circulation on the rotor.

It is easy to see that the induced downwash $W(R)$ increases monotonically, from zero at the hub to a maximum value at the tip, the latter value depending on the parameter λ. Equation (2) shows as $\lambda \to 0$, $W(R)$ has a linear spanwise distribution. Also $W(R)$ vanishes as $\lambda \to \infty$ (infinite blade aspect ratio), and, thus, in this case, the rotary wing is equivalent to a semi-infinite wing.

The blade circulation is given by

$$\Gamma = \Gamma^*/\Omega ac = \pi\alpha_0[R - W(R)] \tag{3}$$

This outer solution, already described, is not valid near the rotor tip, and proper treatment of this irregularity requires consideration of the inner expansion.

Consider the flow in the tip region shown on Fig. 1. In the tip region, the most recently shed trailing vortices can be approximated as straight lines because here the curvature of the trailing vortices is much less than the length scale c. Therefore, their influence is represented by the integral term in Eq. (1). However, different from the fixed-wing case, the previously shed vortices do not remain in the rotor tip-path plane; instead, they are driven downward away from the rotor tip-path plane and form the helical rotor wake. Therefore, the influence of the helical rotor wake needs to be considered in Eq. (1).

We replace U_∞ and y^* in Eq. (1) with Ωr and r, respectively, and nondimensionlize Eq. (1) by writing $R = r/a$. Hence,

$$\Gamma(R) = \frac{mC(R)}{2}\left(\alpha_0 R - \frac{A^{-1}}{4\pi}\int_0^1 \frac{\mathrm{d}\Gamma}{\mathrm{d}R_0}\frac{\mathrm{d}R_0}{R-R_0}\right) \tag{4}$$

where $C(R) = 1$ for a rectangular rotor and Γ has been defined earlier.

To focus on the tip region, we make the transformation $Y = (1-R)A^\beta$, where β is a constant. Substituting Y into Eq. (4), we find, to balance both sides, $\beta = 1$. If we assume that Γ remains $\mathcal{O}(1)$ near the rotor tip, and the chord is finite at the wing tip, then Γ may be expanded as $\Gamma = \Gamma_1 + \mathcal{O}(A^{-1})$. When substituted into Eq. (4), the leading-order terms of the lifting-line integral equation for a semi-infinite wing are found, as

$$\Gamma_1(Y) = \frac{m}{2}\left(\alpha_0 - \frac{1}{4\pi}\int_0^\infty \frac{\mathrm{d}\Gamma_1}{\mathrm{d}Y_0}\frac{\mathrm{d}Y_0}{Y-Y_0}\right) \tag{5}$$

For the helical rotor wake, the correction to the downwash in the tip region, caused by the wake, must be included in Eq. (5). There results

$$\Gamma_1(Y) = \frac{m}{2}\left[\alpha_0 - \frac{1}{4\pi}\int_0^\infty \frac{\mathrm{d}\Gamma_1}{\mathrm{d}Y_0}\frac{\mathrm{d}Y_0}{Y-Y_0} - \alpha_0 W(Y)\right] \tag{6}$$

where $W(Y)$ is the downwash induced by the helical rotor wake in the inner region.

Expanding the outer solution for the downwash in the rotor-tip path plane $W(R)$ in Eq. (2) with the inner variable $Y = (1-R)/A^{-1}$, we find that to leading order as $A \to \infty$

$$W_0(Y) \sim \sqrt{1+8\lambda}\big/4\lambda - 1/4\lambda \tag{7}$$

Substituting $W_0(Y)$ into Eq. (6), we have

$$\Gamma_1(Y) = \frac{m}{2}\left[\alpha_0\left(1 - \frac{\sqrt{1+8\lambda}}{4\lambda} + \frac{1}{4\lambda}\right) - \frac{1}{4\pi}\int_0^\infty \frac{\mathrm{d}\Gamma_1}{\mathrm{d}Y_0}\frac{\mathrm{d}Y_0}{Y-Y_0}\right] \tag{8}$$

When Eq. (8) is compared with the leading-order equation for a fixed wing, it is easy to see that, to leading order, the only difference is the appearance of a constant parameter

$$D = 1 - \sqrt{1+8\lambda}\big/4\lambda + 1/4\lambda$$

which contains the wake information. Therefore, to leading order, in the tip region, a rotary wing is similar to a fixed wing, and thus, Eq. (8) has an analytical solution similar to that of Stewartson.[13]

Hence, Eq. (8) becomes

$$\Gamma_1(Y) = \frac{m\alpha_0 D}{2}\left[1 - \frac{1}{4\pi\alpha_0 D}\int_0^\infty \frac{\mathrm{d}\Gamma_1}{\mathrm{d}Y_0}\frac{\mathrm{d}Y_0}{Y-Y_0}\right] \tag{9}$$

Let $Y = (m/8)\xi$, and let

$$f(\xi) = \frac{2}{\pi m\alpha_0 D}\int_0^\infty \frac{\mathrm{d}\Gamma_1}{\mathrm{d}\xi_0}\frac{\mathrm{d}\xi_0}{\xi-\xi_0} \tag{10}$$

Hence, for the leading-order inner solution, we have

$$\Gamma_1(Y) = (m\alpha_0 D/2)[1 - f(\xi)] \tag{11}$$

and from Eq. (10), the solution is obtained in the same form as that of Stewartson,[13] that is,

$$f(\xi) = \frac{1}{\pi}\int_0^\infty \frac{\exp(-t\,\xi)}{(1+t^2)^{\frac{3}{4}}}\exp\left(-\frac{1}{\pi}\int_0^t \frac{\log\theta\,\mathrm{d}\theta}{1+\theta^2}\right)\mathrm{d}t \tag{12}$$

We call Eq. (11) the modified Stewartson's solution because it is identical to his analytical solution, aside from the parameter D.

Because the bound circulation directly influences the subsequent position of the tip vortex and the intensity of the subsequent interactions with other components of the wake, it is important to determine the circulation as precisely as possible. In the next section, we use lifting-surface theory to evaluate the inner solution, valid near the rotor tip, and compare the results with our lifting-line theory.

Lifting Surface

Following the work of Falkner[21] and of Schlichting and Thomas,[22] the semi-infinite wing may be represented by vortex panels distributed over its surface, as shown in Fig. 4a. For clarity, in Fig. 4a,

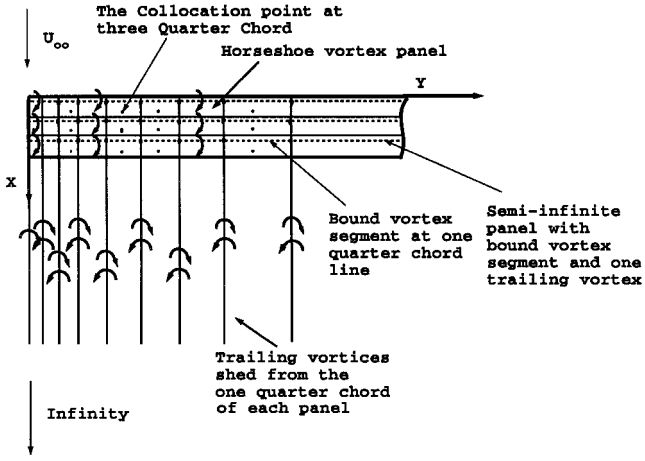

a) Global coordinates

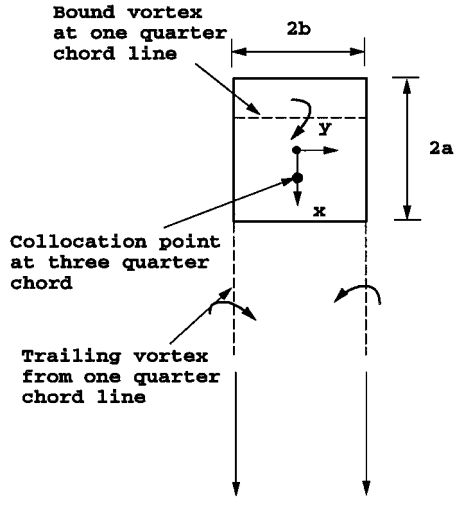

b) Local panel coordinates

Fig. 4 Definitions, where solid box is a surface panel, which is replaced by a horseshoe vortex (– – –).

only three chordwise panels and nine spanwise panels including semi-infinite panels (discussed subsequently) are shown, whereas in the numerical calculation, 10 chordwise and 20 spanwise panels were used. Each wing panel consists of a horseshoe vortex system with a bound vortex along the panel quarter-chord line together with trailing vortices lying along the panel edges, extending through the trailing edge of the wing and moving with the local velocity after leaving the trailing edge of the wing. Figure 4b shows a wing surface panel represented by a horseshoe vortex.

We now define local panel-based coordinates: Define the x axis to be oriented in the chordwise direction, the y axis spanwise, and the z axis vertical, as shown in Fig. 4b. Here x' and y' are measured from the midpoint of the selected panel and z from the plane of the wing. The panel-width dimensions are $2a$ by $2b$ in the chordwise and spanwise directions, respectively. Then the velocity induced by each horseshoe vortex segment is evaluated using Biot–Savart law. The velocity induced by the bound-vortex segment is

$$u_B(x', y', z) = \frac{1}{4\pi}\frac{z}{(x'+a/2)^2+z^2} \times \left[\frac{y'+b}{\sqrt{(x'+a/2)^2+(y'+b)^2+z^2}} - \frac{y'-b}{\sqrt{(x'+a/2)^2+(y'-b)^2+z^2}}\right]$$

$$w_B(x', y', z) = -\frac{1}{4\pi}\frac{x'+a/2}{(x'+a/2)^2+z^2} \times \left[\frac{y'+b}{\sqrt{(x'+a/2)^2+(y'+b)^2+z^2}} - \frac{y'-b}{\sqrt{(x'+a/2)^2+(y'-b)^2+z^2}}\right]$$

whereas the two unit trailing vortices produce the contributions

$$v_{T_1}(x', y', z) = \frac{1}{4\pi}\frac{z}{(y'+b)^2+z^2} \times \left[\frac{x'+a/2}{\sqrt{(x'+a/2)^2+(y'+b)^2+z^2}}+1\right]$$

$$w_{T_1}(x', y', z) = \frac{-1}{4\pi}\frac{y'+b}{(y'+b)^2+z^2} \times \left[\frac{x'+a/2}{\sqrt{(x'+a/2)^2+(y'+b)^2+z^2}}+1\right]$$

and

$$v_{T_2}(x', y', z) = \frac{-1}{4\pi}\frac{z}{(y'-b)^2+z^2} \times \left[\frac{x'+a/2}{\sqrt{(x'+a/2)^2+(y'-b)^2+z^2}}+1\right]$$

$$w_{T_2}(x', y', z) = \frac{1}{4\pi}\frac{y'-b}{(y'-b)^2+z^2} \times \left[\frac{x'+a/2}{\sqrt{(x'+a/2)^2+(y'-b)^2+z^2}}+1\right]$$

where u, v, and w are the x, y, and z components, respectively. Subscript B designates the bound-vortex segment and T_1 and T_2 designate the two trailing vortices.

Now we consider the global coordinates: Define the x axis to be oriented in the chordwise direction, originating at the leading egde of the wing; the y axis spanwise, originating at the wing tip; and the z axis vertical, as shown on Fig. 4a. The panel-influence coefficients A_{kj} are given by the normal velocity induced in the plane of the wing at the three-quarter chord position on panel k due to the horseshoe vortex of unit circulation with the bound vortex at the one-quarter chord position on panel j, as

$$A_{kj} = w_B(x_{kj}, y_{kj}, 0) + w_{T_1}(x_{kj}, y_{kj}, 0) + w_{T_2}(x_{kj}, y_{kj}, 0)$$

where $x_{kj} = x_k - x_j + a/2$ and $y_{kj} = y_k - y_j$. Note x_k, x_j, y_k, and y_j are global variables, and x_{kj}, and y_{kj} are the earlier local variables x' and y'.

The boundary condition of zero normal velocity on the wing surface is satisfied at the three-quarter chord point on the centerline of each panel, as by Schlichting and Thomas,[22] and the vortices emanate from the panel quarter-chord line and extend through the trailing edge of the wing to infinity downstream (Fig. 5). Thus, the panel circulations Γ_k, $k = 1, \ldots, N$, may be evaluated from the surface boundary condition, expressed as the linear equation

$$\sum_{j=1}^{N} A_{kj}\Gamma_j = -\boldsymbol{w}_\infty$$

For a flat-plate airfoil, the right side vector $\boldsymbol{w}_\infty$ is just the vertical component of the freestream velocity vector reduced by the leading-order inner downwash induced by the helical rotor wake, that is, $U_\infty\alpha_0[1 - W_0(Y)]$ in linearized theory.

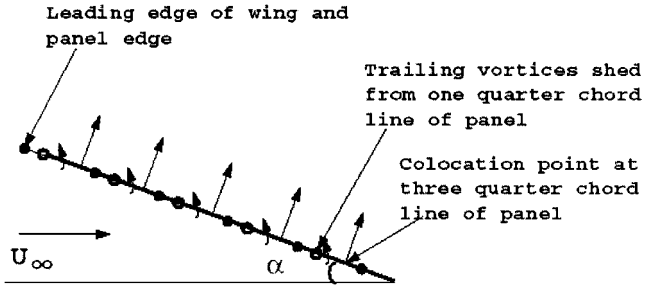

Fig. 5 Schematic of the trailing vortex system: ○, quarter-chord location of each panel (bound vortices); ●, panel edges; and arrows normal direction at the panel three-quarter chord line (normal-velocity boundary condition).

For the numerical computation, the semi-infinite wing is represented by a finite number of panels outboard of a semi-infinite panel. The baseline configuration uses 20 chordwise panels and 40 spanwise panels. The semi-infinite panels have been applied beyond the 40th spanwise panel at each chordwise location to model the semi-infinite aspect of the problem. Each of the semi-infinite panels has only one bound vortex and one trailing vortex, that is, half of a horseshoe vortex. The bound vortex extends to infinity spanwise, and the trailing vortex extends to infinity downstream as shown, in Fig. 4a. The boundary condition of finite circulation at infinity is represented by requiring the values of bound circulation of each of the semi-infinite panels to be equal to those of the panels next to them. The velocities induced by the leading bound-vortex segment of the semi-infinite panel are

$$u_{B\infty}(x, y, z) = \frac{1}{4\pi}\frac{z}{(x + a/2)^2 + z^2} \times \left[1 - \frac{y + b}{\sqrt{(x + a/2)^2 + (y + b)^2 + z^2}}\right]$$

$$w_{B\infty}(x, y, z) = -\frac{1}{4\pi}\frac{x + a/2}{(x + a/2)^2 + z^2} \times \left[1 - \frac{y + b}{\sqrt{(x + a/2)^2 + (y + b)^2 + z^2}}\right]$$

The trailing vorticity becomes small at a distance of the order of a chord length from the wing tip. Hence, accurate computation of the trailing vorticity requires a strong concentration of the horseshoe-vortex panels in the region near the wing tip. Consequently, it is helpful to use panels of variable width. We have chosen the variation

$$y = \bar{b}\tan\theta, \qquad 0 < \theta < \pi/2$$

where $\bar{b}$ is the computational span of the semi-infinite wing. Thus, distributing the panels uniformly in the θ variable increases the physical density of panels near the wing tips. A constant chordwise width was used for each panel because varying panel width was found to be less important in the chordwise variable x.

Figure 6 shows the effect of the number of panels used in the lifting surface code. Note that the comparison is good. This suggests that 10 chordwise panels and twenty spanwise panels are sufficient for the computations.

Figure 7 shows the results of the lifting-surface computation for the bound circulation near the rotor tip. Note the excellent comparison of the numerical results with the modified formula of Stewartson,[13] Eq. (11). Computational results are for 10 chordwise and 20 spanwise panels. In the region of sharp dropoff of the bound circulation, the individual vortex filaments will roll around each other to form the tip vortex. In the region away from the tip, where the circulation approaches a constant, no trailing vorticity is shed to leading order. Comparisons between lifting line and lifting surface models for a finite length rotor blade have been presented by

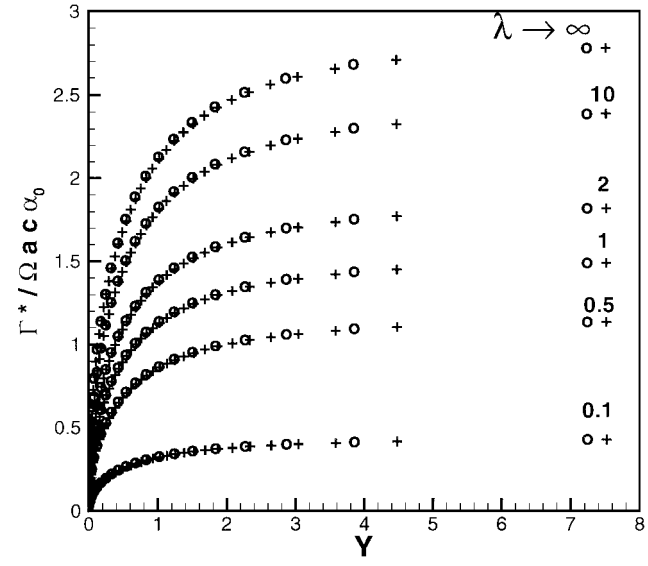

Fig. 6 Comparison of the computational results with different number of panels in the lifting surface code: ○, computational results with 10 chordwise and 20 spanwise panels and +, computational results with 20 chordwise and 40 spanwise panels.

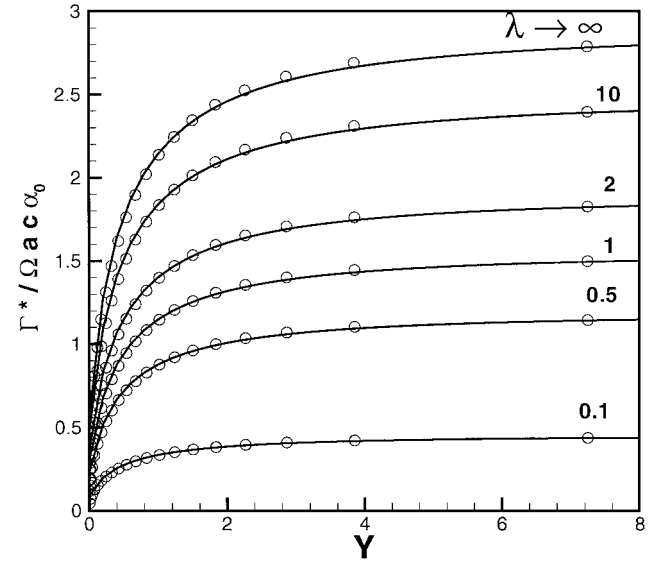

Fig. 7 Comparison of the inner solution for the bound circulation for a rotary wing between the lifting surface code and the modified Stewartson's[13] Eq. (11) indicated by the ——.

Kocurek et al.[23]; they find that lifting-line theory overpredicts the torque coefficient at large thrust coefficient.

Having described the model for the rotor blade, we can calculate the positions of the shed vortices behind the rotor blade. The amount of trailing circulation is determined by the derivative of the bound circulation, and in discrete form the trailing circulation at a fixed radial location in the inner region near the blade tip is

$$\Gamma_t = -\frac{\mathrm{d}\Gamma_B}{\mathrm{d}Y} \tag{13}$$

In a steady inviscid flowfield, the trailing vortex lines are also streamlines. Therefore, we can obtain the positions of vortex lines by solving the set of equations

$$\frac{\mathrm{d}Y}{\mathrm{d}x} = V_0 \tag{14}$$

$$\frac{\mathrm{d}z}{\mathrm{d}x} = \alpha_0[1 - W_0(Y)] \tag{15}$$

where we have linearized the right-hand side of each equation about the dimensionless freestream speed. Here (x, Y, z) are global coordinates, with x measured from the leading edge and nondimensionalized by the chord. Here x is the independent variable measured from leading edge of the wing. The vortices are initiated at the one-quarter chord position of each panel at the beginning of the numerical integration for every iteration. For the initial condition, $z = 0$ and Y is the spanwise location of the trailing vortex shed from the one-quarter chord of each panel. The trailing vortices are forced to stay on the wing surface up to the trailing edge of the wing but can be displaced in the Y direction by the induced velocity, unlike the previous work of the present authors.[24] This set of ordinary differential equations was solved numerically by the Adams–Moulton method. Note that the velocity components were calculated for straight-line trailing vortices in the first iteration.

To obtain the initial positions of the trailing vortices, we introduce three parameters to describe the rollup process. They are $\bar{Y}$ and $\bar{z}$, which are the Y and z components of the center of the tip-vortex core, and $\bar{r}$, which defines the core radius measured from the centroid. We define

$$\bar{Y} = \frac{\sum_{k=1}^{n}\sum_{j=1}^{M}\Gamma_{t,jk}Y_{jk}}{\sum_{k=1}^{n}\sum_{j=1}^{N}\Gamma_{t,jk}} \tag{16}$$

$$\bar{z} = \frac{\sum_{k=1}^{n}\sum_{j=1}^{M}\Gamma_{t,jk}z_{jk}}{\sum_{k=1}^{n}\sum_{j=1}^{N}\Gamma_{t,jk}} \tag{17}$$

where n is the number of trailing vortices which are rolling over each other, M is the number of chordwise panels and Γ_{jk} is the circulation of the panel (j, k). The core radius r has been defined as

$$\bar{r} = \sqrt{\frac{\sum_{k=1}^{n}\sum_{j=1}^{M}(\bar{Y} - Y_{jk})^2 + (\bar{z} - z_{jk})^2}{n \times N}} \tag{18}$$

The iterative process was assumed to be convergent when $(\bar{r}_{\text{new}} - \bar{r}_{\text{old}})/\bar{r}_{\text{old}}$ is less than 10^{-4} at each given value of x. Here we have used one chordwise panel, 20 spanwise panels on the wing surface, and 120 nodes on each of the trailing vortices. The separation between the nodes on each of the trailing vortices is 0.05. Beyond the last node, the trailing vortex is represented by a semi-infinite, horizontal straight vortex line extending to $x = +\infty$ and parallel to the free-stream velocity.

Simple Contraction Model

A simple model for the slipstream contraction has been used to determine the effect of contraction on the bound circulation. In this model, the slipstream has been modeled by a piecewise-continuous sequence of vortex cylinders having different (finite) lengths l_i and radii a_i. The cylinders are distributed both radially and axially to give a discretized representation of the continuous distribution of vorticity in the rotor slipstream. The contraction ratio of successive vortex cylinders is represented by the variable $\delta_i = a_{i+1}/a_i$, $i = 1, \ldots, N$, with $\delta_i < 1$. The first vortex cylinder, $i = 1$, originates in the rotor tip-path plane $z = 0$ and has radius a equal to that of the rotor. The last vortex cylinder, $i = N$, extends downward to infinity. Thus, the overall contraction ratio is a_N/a_1.

For this model, the lifting-line model was solved by a numerical scheme, using the elliptic-integral formulas to follow to evaluate the downwash induced by each vortex cylinder. The slipstream configuration used in the computations, shown in Fig. 8, is composed of 30 vortex cylinders.

The axial velocity induced by a cylinder of radius r' and length $(z_{i+1} - z_i)$, composed of vortex rings of azimuthal vorticity $\gamma_{\theta i}$, may be written as follows[25]:

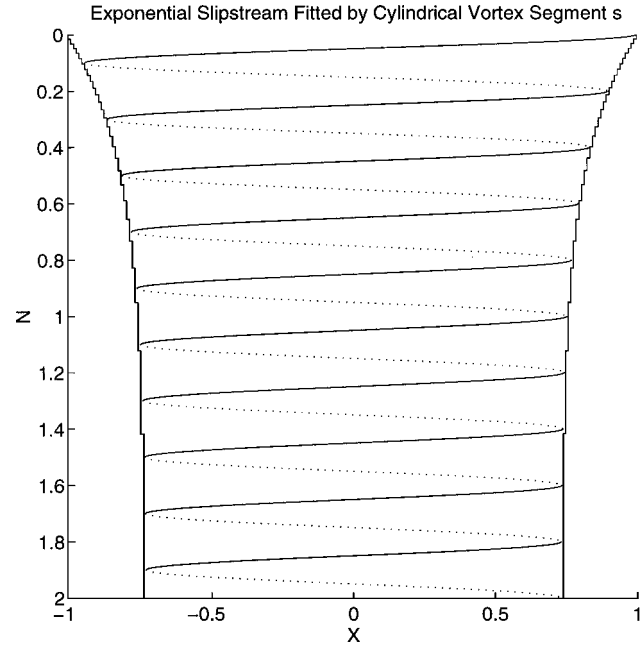

Fig. 8 Exponentially shaped slipstream fitted by cylindrical vortex segments; spirals are for illustrative purposes.

$$v_{z_i}'(r, z; r', z_i, z_{i+1}) = \frac{\gamma_{\theta i}(r')}{2\pi}\left\{\frac{z - z_i}{\sqrt{(z - z_i)^2 + (r + r')^2}}\right.$$
$$\times\left[K(k_{i,i}) - \frac{r - r'}{r + r'}\Pi\left(\sigma_i{}^2, k_{i,i}\right)\right] - \frac{z - z_{i+1}}{\sqrt{(z - z_{i+1})^2 + (r + r')^2}}$$
$$\left.\times\left[K(k_{i,i+1}) - \frac{r - r'}{r + r'}\Pi\left(\sigma_i{}^2, k_{i,i+1}\right)\right]\right\} \tag{19}$$

where K is the complete elliptic integral of the first kind and Π is the complete elliptic integral of the third kind. The moduli of the elliptic integrals are defined as

$$k_{ij}^2 = \frac{4rr'}{(r + r')^2 + (z - z_j)^2}, \qquad \sigma_i^2 = \frac{4rr'}{(r + r')^2}$$

For the uncontracted slipstream, the vortex cylinder is semi-infinite in length. For this limit, the following properties of the elliptic integrals are convenient:

$$K(0) = \pi/2, \qquad \Pi(\sigma^2, 0) = \pi\Big/2\sqrt{1 - \sigma^2}$$

$$\Pi(\sigma^2, \sigma) = E(\sigma)/(1 - \sigma^2)$$

Hence, in the limit $z_i \to 0$, $z_{i+1} \to \infty$, Eq. (19) yields the following result for the axial velocity induced by the uncontracted slipstream:

$$v_z(r, z) = (\gamma_\theta/4)([1 + \text{sign}(a - r)] + (2/\pi)\{z/[(r + a)^2 + z^2]\}$$
$$\times\{K(k) - [(r - a)/(r + a)]\Pi(\sigma^2, k)\}) \tag{20}$$

This result may be used also for the final vortex cylinder of the contracted slipstream model by replacing r by a_N and z by $z - z_N$.

The induced axial velocity for all elementary vortex cylinders, both axially and internally (across the slipstream), is obtained by integrating that for a single cylinder, Eq. (19), with respect to r'

from the axis to the slipstream boundary $r = a_i$, and summing with respect to i over all axial cylindrical segments:

$$v_z(r, z) = \sum_{i=1}^{N} \int_0^{a_i} v'_{z_i}(r, z;\ r', z_i, z_{i+1})\, \mathrm{d}r'$$

The azimuthal vorticity γ_i is equivalent to the strength of the circulation shed from the rotor divided by the axial distance the shed vortex advances in one turn of the rotor. Denote the physical value of the circulation of the shed vortices by Γ_w^*. Then, for small helix angle,

$$\gamma_{\theta i} = \frac{\Gamma_w^*}{v_z \cdot \Delta t} = \left.\frac{\Gamma_w^* \Omega}{2\pi v_z}\right|_{r=r'} \tag{21}$$

Because the circulation of each of the vortex "helices" is constant along the whole length of the slipstream, γ_θ varies inversely with v_z. Because the elementary slipstreams are streamtubes, this implies that γ_θ is proportional to the local radius of the slipstream. Hence the ratio of vorticity of successive vortex cylinders is just

$$\gamma_{\theta i+1} \big/ \gamma_{\theta i} = a_{i+1}/a_i$$

and this result holds for each internal vortex cylinder as well.

The azimuthal vorticity of the uppermost vortex cylinder can be evaluated in terms of the downwash in the rotor path plane as follows. For a thin, uncambered airfoil section, the lift coefficient is given by $C_l = 2\pi\alpha$, where α is the local angle of attack with respect to the relative wind, that is, $\alpha = \alpha_0 - v_z/\Omega r$. Then from the Kutta–Koukowsky theorem, the blade circulation is given by

$$\Gamma^* = \pi c[\Omega\alpha_0 r - v_z]$$

The circulation shed from the blade at radius r, per unit span, is $\Gamma_w^* = \mathrm{d}\Gamma^*/\mathrm{d}r$, so that from Eq. (21) the azimuthal vorticity becomes

$$\gamma_{\theta 1} = \frac{\Omega c}{2a}\frac{1}{W}\left[1 - \frac{\mathrm{d}W}{\mathrm{d}R}\right]$$

where the nondimensional variable R and W have been defined earlier in the lifting-line section. If the downwash is approximated by Eq. (2), then the azimuthal vorticity of the uppermost vortex cylinder is given by

$$\gamma_{\theta 1} = (2\Omega c\lambda/a) \cdot \left(1\Big/\sqrt{1 + 8\lambda R}\right)$$

The streamtube induced by the semi-infinite (uncontracted) vortex cylinder provides a convenient approximation for the shape of the contracted slipstream. The coordinates of the streamtube were obtained by integrating the equation for its slope:

$$\frac{\mathrm{d}r}{\mathrm{d}z} = \frac{v_r}{v_z}$$

where the radial and axial components of velocity are obtained from elliptic-integral formulas corresponding to Eq. (20), as given by Radcliff et al.[25] The results closely fit the exponential approximation

$$R = R_1 + (1 - R_1)\exp(-Z/Z_1)$$

where $R_1 = 0.729$ and $Z_1 = 0.4254$. Note that R and Z are normalized by the rotor tip radius, as defined earlier in the lifting-line section. In the calculations, the radii a_i of the outermost vortex cylinders were evaluated from this exponential approximation.

Results

No Wake Contraction

In this section, results will be presented first for the bound circulation and then for the rollup process. As mentioned, we solve for the bound circulation on the rotor by the method of matched

Table 1 Parameters for the rotor investigated by McAlister et al.[10]

Parameter	Value
R	1.14 m
ΩR	132 m/s
n_b	2
Chord	0.191 m
Attack angle	8 deg

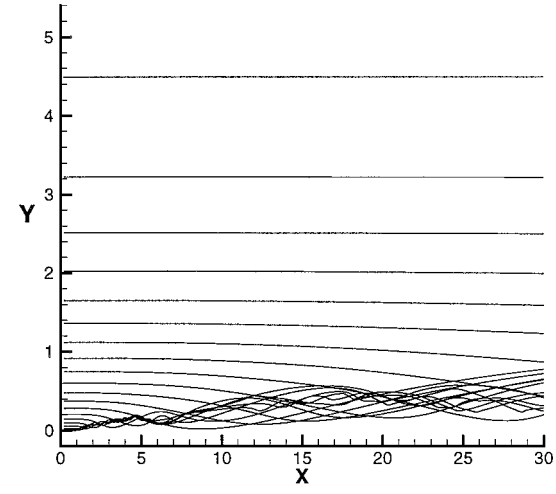

a) Plan view

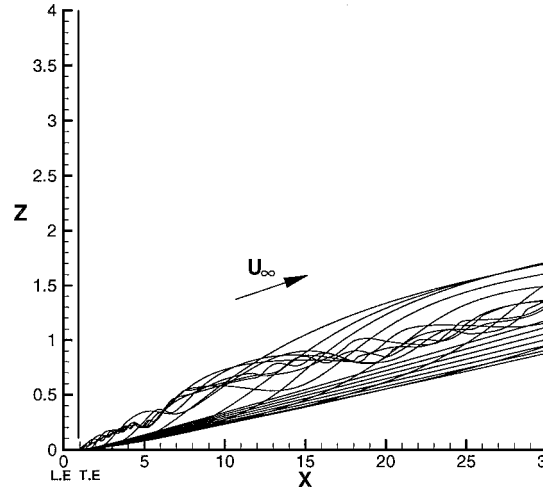

b) Radial view

Fig. 9 Section view of rollup process of trailing vortices shed from the rotor; core radius converges up to $x = 30$, angle of attack is 8 deg, and single chordwise panel used.

aymptotic expansion. We use "mutiplicative composition," as defined by Van Dyke,[12] to form the uniformly valid solution for the bound circulation

$$\Gamma_{\text{uniform}} = \frac{\Gamma_{\text{inner}} \times \Gamma_{\text{outer}}}{\Gamma_{\text{cp}}} \tag{22}$$

where Γ_{inner} is the inner solution of the bound circulation (near the tip region) given by the modified Stewartson[13] or the lifting surface code, Γ_{outer} is the outer solution,[26] and Γ_{cp} is the common part, which is defined as the bound circulation evaluated either in the limit as the outer variable $R \to 1$ or as the inner variable $Y \to \infty$.

The parameters of the rotor are are chosen to correspond to the parameters of McAlister et al.[10] and are given in Table 1. Figures 9a and 9b present the x–Y and x–z views of the rollup process for the rotor, which converges up to $x = 30$. The vortex lines emanating from each panel are shown here. The direction of U_∞ relative to the rotor blade is indicated. Note that the trailing vortices near the

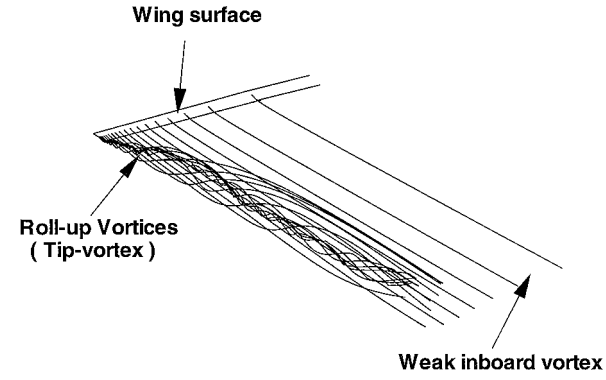

Fig. 10 Three-dimensional view of the rollup process of the trailing vortices; angle of attack 8 deg, single chordwise panel used, and iteration process converges up to $x = 30$.

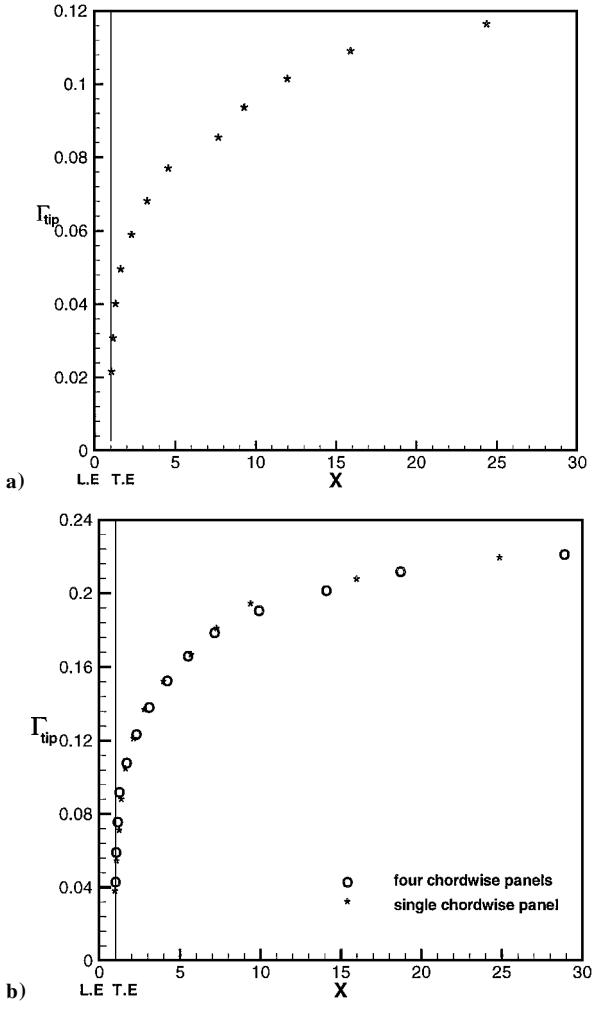

Fig. 11 Evolution of the circulation of the tip vortex: a) angle of attack is 8 deg, maximum bound circulation is 0.153, core radius has converged up to $x = 30$, and single chordwise panel used and b) angle of attack is 12 deg and maximum bound circulation is 0.274.

tip region roll over and form a strong trailing vortex. However, in the region away from the tip, the trailing vortices do not rollup in distances of the order shown here. The tip vortex is also shown to have moved inboard. The three-dimensional view is presented in Fig. 10.

Figure 11 shows the growth of the circulation of the tip vortex as a function of x. The circulation of the tip vortex is obtained by summing the circulations of each of the individual filaments. The open circles in Fig. 11 are the solution using four chordwise panels. For the rotor at $\alpha_0 = 8$ deg seen in Fig. 11a, as we go farther downstream, and the iteration process is converged to $x = 30$, the circulation of the tip vortex has reached 79% of the maximum bound circulation. The asterisks in Fig. 11 are the solution for a single chordwise panel that is very close to four panel case. Clearly, one panel is sufficient for design purposes, a big savings in computational cost.

Figure 12 shows the downstream development of the core radius $\bar{r}$ of the tip vortex measured from the centroid for angle of attack

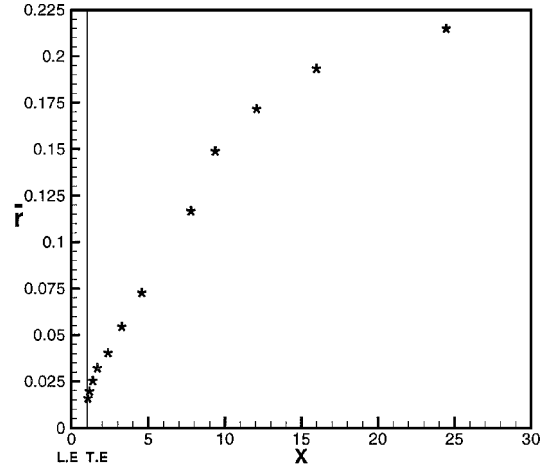

Fig. 12 Evolution of the core radius $\bar{r}$ of the tip vortex measured from the centroid; core radius has converged up to $x = 30$, single chordwise panel is used, and angle of attack is 8 deg.

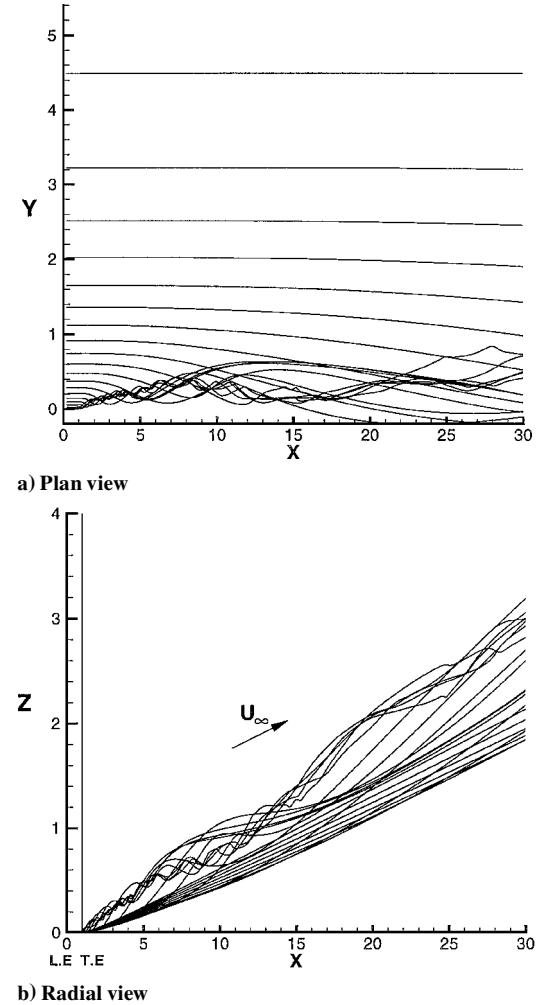

Fig. 13 Section view of the rollup process of trailing vortices shed from the rotor; core radius converges up to $x = 30$, angle of attack is 12 deg, and single chordwise panel is used.

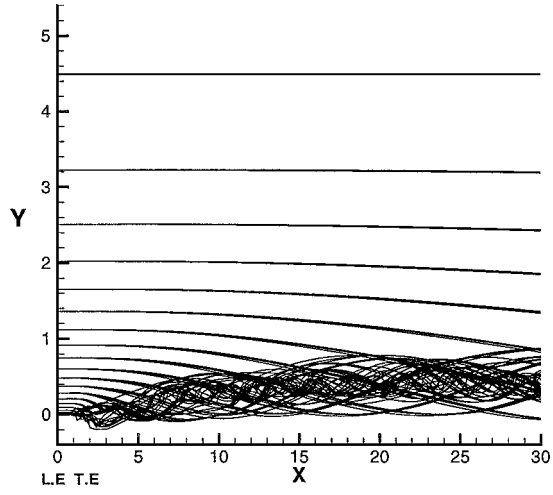

a) Plan view

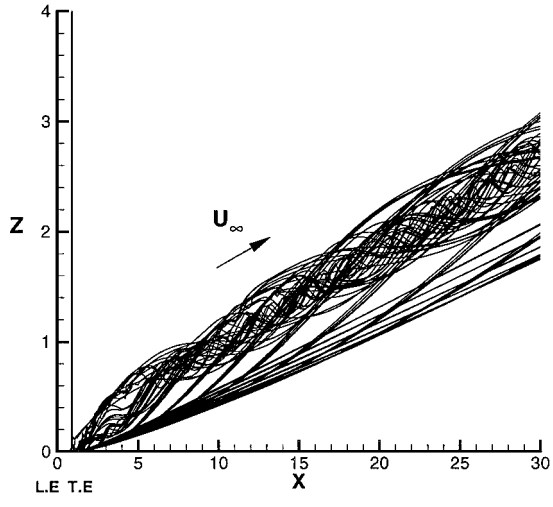

b) Radial view

Fig. 14 Section view of rollup process of trailing vortices for a rotary wing; iteration process converges up to $x = 30$, and angle of attack is 12 deg.

of 8 deg. The core radii $\bar{r}$ in Fig. 12 were calculated at each downstream location x at which an additional trailing vortex enters the rolling-over trailing vortices. Note that $\bar{r}$ develops downstream and approaches a constant asymptotically.

Figures 13a and 13b show the x–Y and x–z views of the rollup process for a rotor with $\alpha_0 = 12$ deg. A single chordwise panel was used in this case. The core radius is converged out to $x = 30$. Note that the center of the core has moved.

Figures 14a and 14b show the x–Y and x–z views of the rollup process for the rotary wing at $\alpha_0 = 12$ deg with 4 chordwise and 20 spanwise panels. Note that trailing vortices shed from different chordwise panels but from the same spanwise location roll into the single strong tip vortex at different downstream locations. The trailing vortices that emanate from the panels closer to the leading edge of the rotor blade roll into the tip vortex more quickly. The three-dimensional view is shown in Fig. 15.

Table 2 shows the comparison of the circulations of the tip vortex for different fixed and rotary wings. At the same angle of attack and downstream location, the tip vortex shed from a fixed wing[24] is stronger than that for a rotary wing, that is, the fixed wing tip vortex develops more quickly than the rotor tip vortex. Morever, the tip vortex shed by the wing at higher angle of attack also develops more quickly than that shed by the wing at lower angle of attack. Such a different downstream development is attributed to the different spanwise variation of the bound circulation near the tip region: A steeper spanwise gradient produces stronger tip vortices and, hence, a quicker development of the tip vortex.

Table 2 Circulation of the tip vortex for different rotary wings[a]

Wing	α_0, deg	x_1	$\Gamma_{tip}/\Gamma_{maxbnd}$
Rotary1	8 deg	30	0.785
Rotary2	12 deg	30	0.815

[a]Two-bladed rotor of aspect ratio six and consisting of a single chordwise panel and 20 spanwise panels is used in each case.

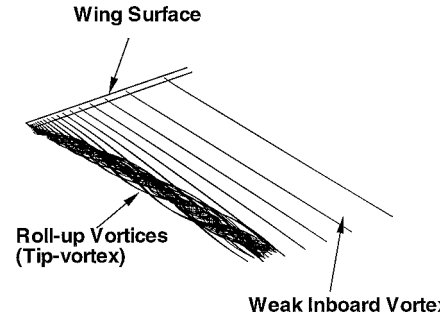

Fig. 15 Three-dimensional view of rollup process of the trailing vortices; angle of attack is 12 deg, 4 chordwise panels and 20 spanwise panels used, and iteration process converges up to $x = 30$.

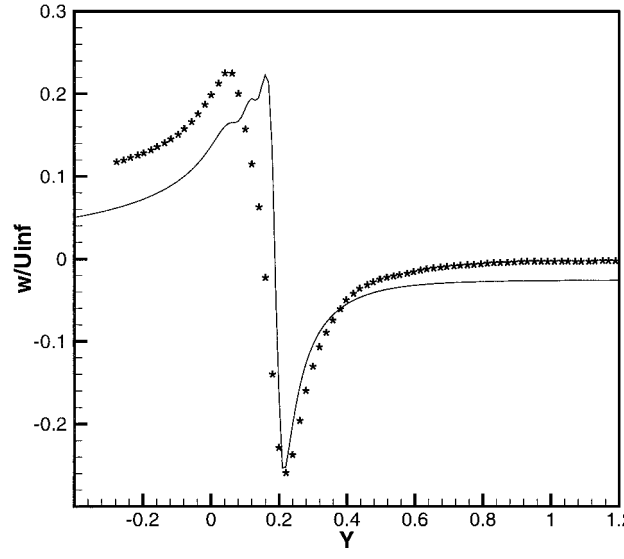

Fig. 16 Vertical velocity in the rotor plane at $x = 4$, three chord lengths behind the trailing edge of the rotor: ∗, is experimental data from McAlister et al.[27]; ——, is computational data; and rotor tip is at $Y = 0$, and inboard locations are for $Y > 0$, 8-deg angle of attack.

Figure 16 compares the numerical results for the vertical velocity with the more recent experimental data of McAlister et al.[27] at a position three chord lengths behind the trailing edge of the rotor. The comparison is surprisingly good, although the spanwise location of the maximum positive velocity occurs inboard of the experimental result.

Effect of Contraction

Consider the downwash induced by the rotor-wake contraction in the inner region, where $R \sim 1$. Li[26] has evaluated the influence of contraction on the value of the downwash, and the maximum deviation from the uncontracted value is 8% for $\lambda = 0.07$ and only 5% for $\lambda = 7$. This influence may be significant from the point of view of blade loading and design, but for the present fundamental study, the influence is considered minor. Consequently, in the results presented here, the influence of contraction was only incorporated in the outer solution for the bound circulation away from the blade tip.

Figure 17 is a comparison of the resulting uniformly valid solution without slipstream contraction with the solution accounting

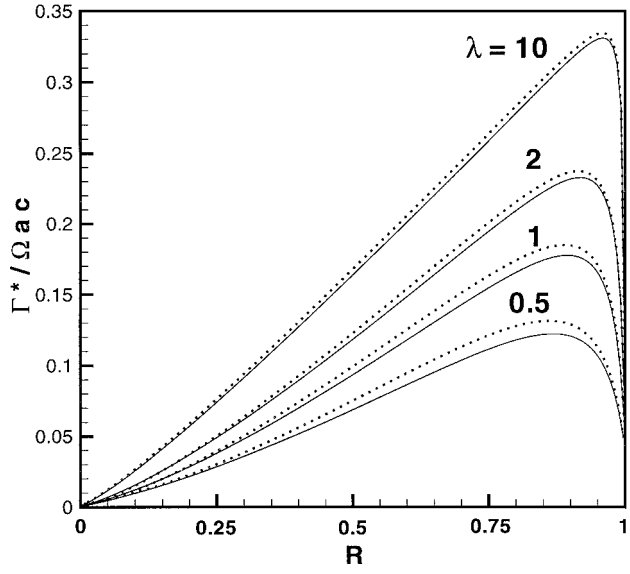

Fig. 17 Uniformly valid solutions with and without wake contraction for different λ, with $\alpha_0 = 8$ deg: · · · ·, without wake contraction and ——, with wake contraction.

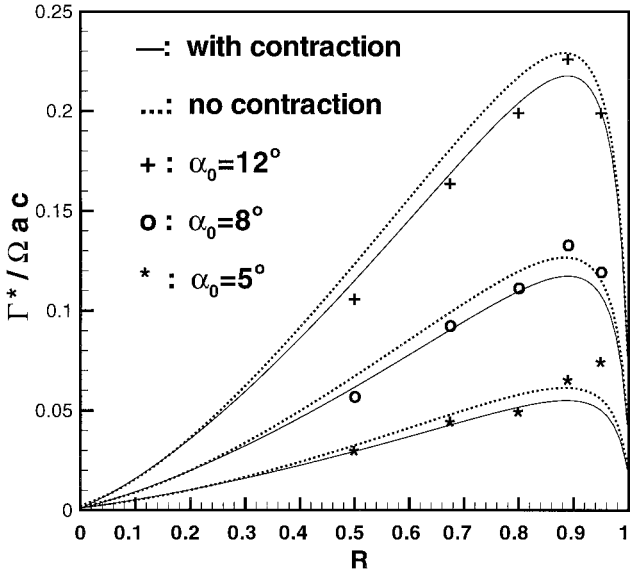

Fig. 18 Comparison of the computational solutions with the experimental data of Caradonna and Tung[9] for a two-bladed rotor: ——, numerical solutions with wake contraction; · · · ·, numerical solutions without wake contraction; +, experimental data for $\alpha_0 = 12$ deg; ○, experimental data for $\alpha_0 = 8$ deg; and ∗, experimental data for $\alpha_0 = 5$ deg.

for the rotor-wake contraction. Note that as λ increases the effect of slipstream contraction is reduced. This effect appears to be due to the reduction of induced downwash with increasing λ.

Figure 18 shows a comparison of the current theoretical results with the experimental data of Caradonna and Tung.[9] The comparison is reasonably good in each case, although the peak value is underpredicted for the smallest value of angle of attack ($\alpha_0 = 5$ deg). For the large angle of attack ($\alpha_0 = 12$ deg), the wake contraction model produces better results than the model without wake contraction except near the tip.

Summary

We have developed a model for the aerodynamics of the formation of a rotary-wing tip vortex based on vortex-dynamics considerations. The flow near the tip of a large aspect ratio rotary wing is equivalent to the flow past a semi-infinite fixed wing with appropriately modified freestream and the incorporation of a suitable wake model. We have presented results for the bound circulation on the wing and for the subsequent rollup and formation of the tip vortex downstream of the blade tip. Following the work of Falkner[21] and Schlichting and Thomas,[22] we have modeled the lifting surface as a distribution of horseshoe vortices. The lifting-surface results compare very well with the analytical solution of Stewartson[13] for the lifting line, suitably modified to account for the rotor wake. Moreover, the solution for the bound circulation does not seem to depend strongly on the number of panels in the chordwise direction, and 20 spanwise panels is sufficient in the spanwise direction.

In the tip region where the bound circulation varies rapidly, the individual vortex segments roll over each other and form a strong tip vortex. The tip vortex does not completely roll up near the rotor, as assumed by many wake models; instead, the tip vortex develops downstream, and its circulation seems to be approaching a constant, which appears to be significantly less that the maximum bound circulation. However, more work needs to be done to confirm this point.

The results for the vertical velocity induced by the shed vorticity compared well with the experimental results of McAlister et al.[10] No turbulence model was necessary despite that, at the Reynolds numbers of the experiment, the flow would be expected to be turbulent. The numerical results for the bound circulation compare well with the experimental data from Caradonna and Tung,[9] and the influence of contraction within the inner region near the blade tip appears to be of second order. Based on the comparisons with experimental data, there is little basis for the argument that the presence of turbulence has a significant effect on the structural properties of the tip vortex.

Acknowledgments

This work has been supported by U.S. Army Research Office and monitored by Thomas L. Doligalski. The authors are grateful for his support during the course of this research. Thanks are due also to Ning Mei, Santosh Kini, and Vishwanath Godavarty, who aided in preparing some of the figures.

References

[1]Jain, R., and Conlisk, A. T., "Interaction of Tip-Vortices in the Wake of a Two-Bladed Rotor in Axial Flight," *Journal of the American Helicopter Society*, Vol. 45, No. 3, 2000, pp. 157–164.

[2]Kini, S., and Conlisk, A. T., "The Development of Steady State Rotor Wakes," American Helicopter Society Aeromechanics Specialists' Meeting, Nov. 2000.

[3]Tung, C., and Lee, S., "Evaluation of Hover Prediction Codes," *Proceedings of the 50th Annual Forum of the American Helicopter Society*, 1994, pp. 829–844.

[4]Tung, C., Yu, Y., and Low, S., "The Aerodynamic Aspects of Blade/Vortex Interaction," AIAA Paper 96-2010, June 1996.

[5]Mahalingam, R., "Experiments on the Origin of Tip Vortices," AIAA Paper 2000-0278, Jan. 2000.

[6]Bhagwat, M. J., and Leishman, G. J., "On the Relationship Between Blade Circulation and Tip Vortex Characteristics," 54th Annual Forum of the American Helicopter Society, May 1998.

[7]Rule, J. A., and Bliss, D. B., "Prediction of Viscous Trailing Structure from Basic Loading Parameters," *AIAA Journal*, Vol. 36, No. 2, 1998, pp. 208–218.

[8]Cook, C. V., "The Structure of the Rotor Blade Tip Vortex," *Aerodynamics of Rotary Wings*, CP-111, AGARD, 1972.

[9]Caradonna, F. X., and Tung, C., "Experimental and Analytical Studies of a Model Helicopter Rotor in Hover," NASA TM 81232, Sept. 1981.

[10]McAlister, K. W., Schuler, C. A., Branum, L., and Wu, J. C., "3-D Measurements Near a Hovering Rotor for Determining Profile and Induced Drag," NASA TP 3577, Aug. 1995.

[11]Van Dyke, M., "Lifting-Line Theory As a Singular Perturbation Problem," *Archiwum Mechaniki Stosowanej*, Vol. 16, No. 3, 1964, pp. 601–614.

[12]Van Dyke, M., *Perturbation Methods in Fluid Mechanics*, anotated ed., Parabolic, Stanford, CA, 1975.

[13]Stewartson, K., "A Note On Lifting Line Theory," *Quarterly Journal of Mechanics and Applied Mathematics*, Vol. 13, Pt. 1, 1960, pp. 49–56.

[14]Head, M. R., "Flow Visualization in Cambridge Univ. Engineering Department," *Flow Visualization II*, edited by W. Merzkirch, Hemisphere, Washington, DC, 1982, pp. 399–403.

[15]Van Dyke, M., *An Album of Fluid Motion*, Parabolic Stanford, CA, p. 51.

[16]Anderson, J. D., *Fundamentals of Aerodynamics*, 2nd ed., McGraw–Hill, 1991, Fig. 5.42, p. 366.

[17] Katz, J., and Plotkin, A., *Low-speed Aerodynamics: from Wing Theory to Panel Methods*, McGraw–Hill, New York, 1991, p. 172.

[18] Knight, M., and Heffner, R. A., "Static Thrust Analysis of the Lifting Airscrew," NACA TN 626, 1937.

[19] Gessow, A., and Myers, G. C., *Aerodynamics of the Helicopter*, Macmillan New York, 1952, p. 68.

[20] Glauert, H., "Airplane Propellers," *Aerodynamic Theory*, edited by W. F. Durand, Vol. 4, Julius Springer, 1943, pp. 169–360.

[21] Falkner, V. M., "The Calculation of Aerodynamic Loading on Surfaces of Any Shape," Reports and Memoranda Aero. Res. Comm., Rept. 1910, Aeronautical Research Communication, London, 1943.

[22] Schlichting, H., and Thomas, H. H. B. M., "Note on the Calculation of Lift Distribution of Swept Wings," Royal Aircraft Establishment, Rept. Aero. 2236, London, 1947.

[23] Kocurek, J. D., Berkowitz, L. F., and Harris, F. D., "Hover Performance Methodology at Bell Helicopter Textron," *Proceedings of the 36th Annual Forum of the American Helicopter Society*, 1980, pp. 80-3-1–80-3-26.

[24] Li, H., Burggraf, O. R., and Conlisk, A. T., "On the Formation of a Tip Vortex," AIAA Paper 2000-0282, 2000.

[25] Radcliff, T. D., Burggraf, O. R., and Conlisk, A. T., "On the Three-Dimensional Interaction of a Rotor-Tip Vortex with a Cylindrical Surface," *Journal of Fluid Mechanics*, Vol. 25, 2000, pp. 301–334.

[26] Li, H., "Formation of Rotor Tip Vortices," M.Sc. Thesis, Dept. of Mechanical Engineering, Ohio State Univ., Columbus, OH, June 2000.

[27] McAlister, K., Tung, C., and Heineck, J. T., "Devices that Alter the Tip Vortex of a Rotor," NASA/TM-2001-209625, AFDD/TR-01-A-003, 2001.